

Photoreceptor Outer Segment Reflectivity With Ultrahigh-Resolution Visible-Light Optical Coherence Tomography in Systemic Hydroxychloroquine Use

Anupam K. Garg^{1,*}, Jingyu Wang^{1,2,*}, Bailee Alonzo¹, Ji Yi^{1,2}, and Amir H. Kashani^{1,3}

¹ Wilmer Eye Institute, Johns Hopkins University, Baltimore, MD, USA

² Department of Biomedical Engineering, Johns Hopkins University, Baltimore, MD, USA

³ Department of Biomedical Engineering, Johns Hopkins Hospital, Baltimore, MD, USA

Correspondence: Amir H. Kashani, Wilmer Eye Institute, Johns Hopkins University, 600 North Wolfe Street, Baltimore, MD 21287, USA. e-mail: akashan1@jhmi.edu

Received: September 5, 2024

Accepted: January 19, 2025

Published: March 3, 2025

Keywords: optical coherence tomography; retinal imaging; hydroxychloroquine

Citation: Garg AK, Wang J, Alonzo B, Yi J, Kashani AH. Photoreceptor outer segment reflectivity with ultrahigh-resolution visible-light optical coherence tomography in systemic hydroxychloroquine use. *Transl Vis Sci Technol.* 2025;14(3):2. <https://doi.org/10.1167/tvst.14.3.2>

Purpose: To evaluate outer retinal organization in normal subjects and those using hydroxychloroquine (HCQ) with ultrahigh-resolution visible-light optical coherence tomography (VIS-OCT).

Methods: Forty eyes of 22 adult subjects were recruited from a tertiary-care retina practice, including controls (20 eyes, 12 subjects, 40 ± 22 years old) and subjects with a history of HCQ use (20 eyes, 10 subjects, 62 ± 17 years old). Each subject was imaged using a custom-built VIS-OCT device (axial resolution 1.3 μm) and U.S. Food and Drug Administration–approved OCT devices.

Results: With the use of VIS-OCT, control subjects demonstrated five and six hyperreflective bands in the foveal and parafoveal regions, respectively, between the outer nuclear layer and Bruch's membrane. These bands demonstrated intensity profiles complementary to the known histopathologic distribution of rods and cones. In comparison to controls, subjects taking HCQ demonstrated reduced intensity of all bands, particularly bands two to four. In all cases of suspected or known toxicity, VIS-OCT demonstrated attenuation of band 3i, and in no cases was there attenuation of other bands that was more severe than band 3i, suggesting that changes in the reflectivity of band 3i may be the earliest identifiable sign of HCQ toxicity.

Conclusions: VIS-OCT of the outer retina revealed a unique outer retinal banding pattern corresponding to photoreceptor density distributions. Notable attenuation of the photoreceptor outer segment reflectivity profile was associated with early HCQ toxicity. This finding may be an early, and possibly reversible, sign of HCQ toxicity, primarily impacting the cones.

Translational Relevance: VIS-OCT is useful in detecting subclinical outer retinal structural changes found in subjects using hydroxychloroquine.

Introduction

Hydroxychloroquine (HCQ) is a well-described anti-inflammatory and antimalarial medication with relatively rare but devastating toxic effects on the retina.¹ Although a benign drug in general, the potential for this serious side effect causes significant problems in the management of patients who are on the medication. The exact pathophysiology of the side effect is not well understood; however, several

lines of evidence suggest that toxicity at the level of the retinal pigment epithelium (RPE) and, secondarily, the photoreceptor is likely. *In vitro* studies have demonstrated that HCQ inhibits protein synthesis² and lysosomal function³ in the RPE. Toxicity manifests in subjects with prolonged HCQ exposure as thinning of the outer retina and loss of the RPE in a bull's-eye pattern.⁴ However, even subjects without any clinical findings or subjective symptoms can demonstrate subclinical signs of toxicity such as modest retinal thinning on optical coherence tomography (OCT) and

decreased signal amplitude on multifocal electroretinogram (mfERG).^{5,6} Based on careful analysis of OCT images, it has been hypothesized that changes in reflectivity in outer retinal bands are imaging correlates of ellipsoid zone (EZ) loss⁷ and/or changes in the photoreceptor outer segments.⁸ Although severe changes may be seen with retinal thickness maps,⁹ the resolution of commercially available OCT devices is not sufficient to easily and reliably assess subclinical changes in the outer segment banding patterns on single OCT volumes.¹⁰ To overcome this limitation, serial OCT imaging has been used to detect very subtle paracentral thinning patterns that seem strongly correlated with toxicity.⁶ This finding suggests that higher resolution imaging of the photoreceptor/RPE complex may reveal even earlier signs of toxicity.

Most commercial devices utilize near-infrared (NIR)-wavelength light with axial resolutions of ~5 to 10 μm , ultrahigh-resolution visible-light OCT (VIS-OCT) utilizes shorter wavelengths of light to enable higher axial resolution (~1 μm).¹¹ Recent technological advances have led to the development of VIS-OCT devices for human retinal imaging, enabling characterization of both inner and outer retinal layers in greater detail than previously possible in human subjects^{12–16} and animal models.^{17,18} Prior work has demonstrated that VIS-OCT reveals outer retinal banding morphology not readily visible with conventional devices in control subjects without a known history of retinal pathology, including Bruch's membrane (BM) and sub-bands in photoreceptor outer segments.¹⁹ Similar banding morphology has also been recently demonstrated using ultrahigh-resolution spectral-domain OCT (SD-OCT) prototype devices.^{20,21} In vivo characterization of these fine details and their changes in retinal disease may provide valuable insights into disease pathophysiology and management. Given that the outer retina is primarily affected in early HCQ toxicity, VIS-OCT is a promising imaging modality to enable early detection of HCQ toxicity. In this study, we used a custom-built VIS-OCT device to identify subtle outer retinal changes in HCQ toxicity not visible with conventional OCT devices.

Methods

Recruitment of Subjects

Both eyes of adult subjects with a history of HCQ use were prospectively recruited from a tertiary-care retina practice for retinal imaging with a custom-built dual-channel VIS-OCT device with an axial resolu-

tion of 1.3 μm (Fig. 1).^{19,22} Each subject was also imaged using a commercial swept-source OCT (SS-OCT) imaging device. The most recent hepatic and renal function testing results of each subject were also obtained. Control subjects were recruited from the retina clinics if they had no vision-threatening retinal or ocular disease in at least one eye. For subjects with a history of hydroxychloroquine (HCQ) use, each subject's HCQ dose and duration of therapy were obtained from the medical chart, if available. The cumulative lifetime dose was calculated by multiplying the dose by the duration of therapy, as shown in the Table. Information regarding subjects is summarized in the Table. All subjects provided informed consent according to a human subject protocol approved by the institutional review board and in accordance with the tenets of the Declaration of Helsinki. Subjects with significant media opacity, poor signal quality, or inability to fixate sufficiently to obtain at least one high-quality foveal line scan were excluded.

Imaging Device

The dual-channel VIS-OCT system features a visible-light bandwidth ranging from 500 to 650 nm and a NIR light bandwidth spanning 750 to 900 nm. The spectral full-width at half maximum (FWHM) for the visible channel is 100 nm, yielding an axial resolution of approximately 1.3 μm in tissue. The FWHM of the NIR channel is 69 nm, achieving an axial resolution of 3.7 μm in tissue. Both channels utilize e2v Octoplus 2048-pixel line scan cameras (Teledyne Vision Solutions, Waterloo, ON, Canada), running at a line rate of 100 kHz. The NIR channel operates with a commercial Cobra-S 800 spectrometer (Wasatch Photonics, Morrisville, NC). The visible-light channel employs a custom-designed linear-in- k spectrometer, which incorporates a diffraction grating (1800 lines/mm) and a prism to optimize spectral resolution and reduce sensitivity roll-off. The incident intensities of each channel were <0.22 mW for VIS-OCT and <0.9 mW for NIR-OCT at the cornea, respectively. Subjects were instructed to fixate using one of two light-emitting diode (LED) displays that served as an external fixation target. A tunable lens was utilized to correct spherical errors. For each eye, the image was initially aligned and optimized under the NIR channel and then promptly imaged with the visible-light channel. Full technical details of the device are available in a previous publication.²²

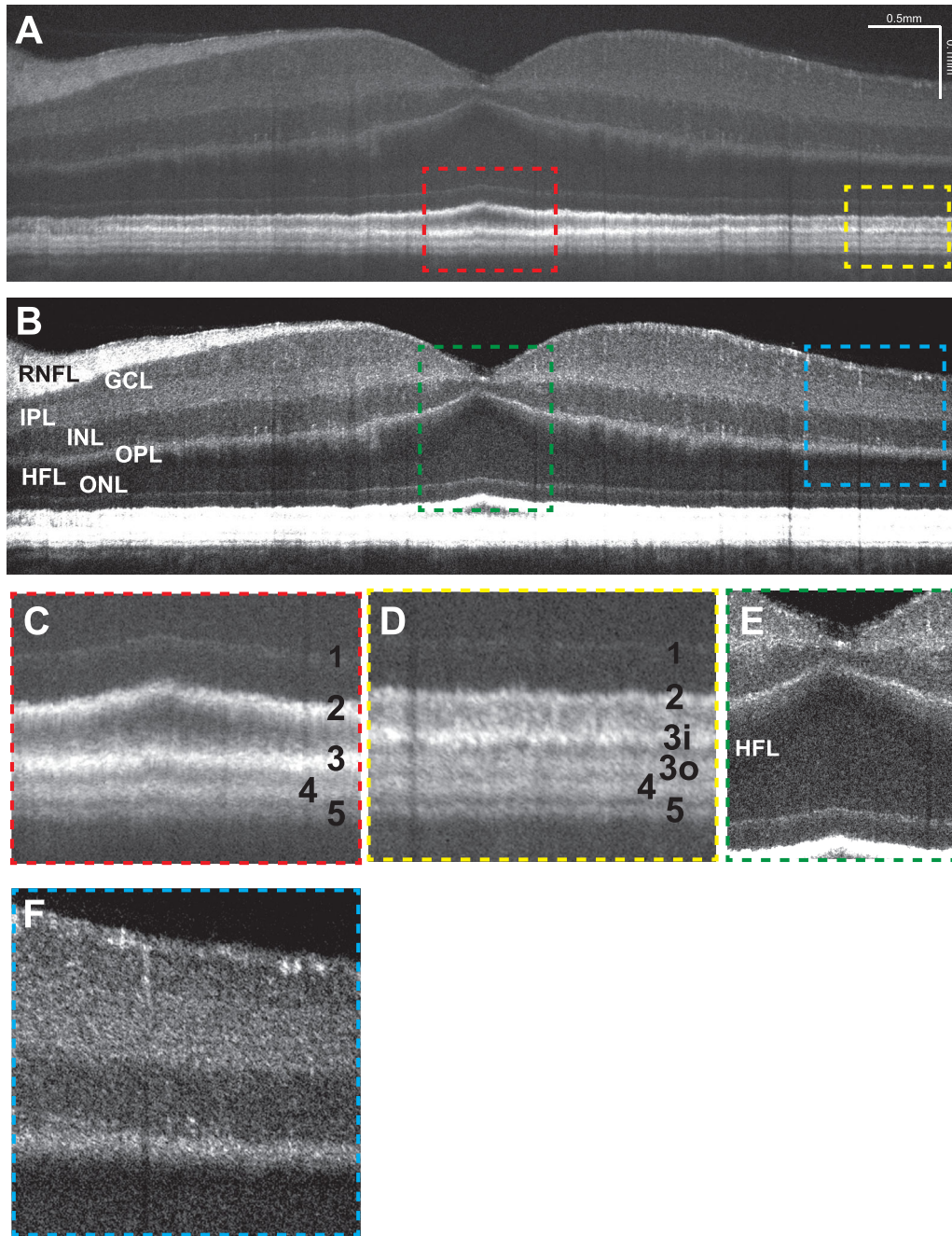


Figure 1. (A) Contrast-adjusted VIS-OCT image of a 35-year-old Caucasian male subject with no known ocular history or retinal pathology highlighting outer retinal features. (B) Contrast-adjusted image highlighting inner retinal features. (C) Magnified view of foveal outer retinal features seen in panel (A) demonstrating the outer retinal banding pattern with outer retinal bands labeled. (D) Magnified view of parafoveal outer retina. (E) Magnified view of foveal inner retinal features seen in panel (C). (F) Magnified view of parafoveal inner retinal features. GCL, ganglion cell layer; HFL, Henle’s fiber layer; INL, inner nuclear layer; IPL, inner plexiform layer; ONL, outer nuclear layer; OPL, outer plexiform layer; RNFL, retinal nerve fiber layer.

Imaging Protocol

All subjects underwent SD-OCT imaging performed with a commercially available device (SPECTRALIS OCT, Heidelberg Engineering,

Heidelberg, Germany; or CIRRUS SD-OCT, ZEISS, Oberkochen, Germany) as part of their standard-of-care assessment. In addition, subjects were scanned using two research OCT devices, including the custom-built, dual-channel, ultrahigh-resolution VIS-

Table. Study Subject Demographics

Subject	Diagnosis	Age (Y)	Race	Sex	Years HCQ Use	Known Toxicity?	Cumulative HCQ Dose, Renal/Hepatic Function	Visual Acuity
271	SLE	66	WNH	F	22	Suspected	3212 g Creatine: 0.9 mg/dL AST/ALT: 25/19 U/L	20/20 OU
308	SLE	66	BNH	F	27	No	4088 g Creatine: 0.89 mg/dL AST/ALT: 25/17 U/L	20/20 OU
178	Sjogren's syndrome and SLE	53	WNH	F	4	Yes	584 g Creatine: 0.56 mg/dL AST/ALT: 29/26 u/L	20/50 OD 20/80 OS
347	RA	76	WNH	F	31	Suspected	4526 g Creatine: 1.5 mg/dL AST/ALT: 26/19 U/L	20/50 OD 20/40 OS
370	Undifferentiated connective tissue disease	33	WNH	F	1	No	146 g Creatine: 0.7 mg/dL AST/ALT: 17/26 U/L	20/20 OU
374	SLE	35	BNH	F	2	No	292 g Creatine: 0.7 mg/dL AST/ALT: 22/20 U/L	20/20 OU
417	RA	76	WNH	F	35	Yes	Unknown cumulative dose Creatine: 0.9 mg/dL AST/ALT: 40/25 U/L	20/50 OD 20/250 OS
439	SLE	62	WNH	F	11	No	1204.5 g Creatine: 1.5 mg/dL AST/ALT: 21/10 U/L	20/20 OU
445	RA and sarcoidosis	84	WNH	M	5	No	730 g Creatine: 0.99 mg/dL AST/ALT: 18/7 U/L	20/40 OD 20/25 OS
378	SLE	73	BNH	F	5	Suspected	730 g Creatine: 0.9 mg/dL AST/ALT: 19/15 U/L	20/25 OU
Subject	Diagnosis	Age (y)	Race	Sex	Eye(s) Imaged	Diagnosis	Visual Acuity	
451	Control	26	BNH	M	OU	N/A	—	
456	Control	23	WNH	F	OU	N/A	20/20 OU	
446	Control	22	WNH	F	OU	N/A	20/20 OU	
464	Control	24	WNH	F	OU	N/A	—	
465	Control	25	BNH	F	OU	N/A	20/20 OU	
402	Control	70	WNH	M	OU	N/A	20/20 OU	
399	Control	26	ANH	F	OD	Optic disc pit OS	20/20 OD	
395	Control	80	WNH	F	OU	PVD OU	20/32 OD 20/25 OS	
385	Control	27	WH	M	OU	N/A	—	
303	Control	63	WNH	F	OD	Choroidal nevus OS	20/32 OD	
409	Control	35	WNH	F	OU	CRVO OS	20/32 OD 20/12.5 OS	
333	Control	59	BNH	M	OU	PVD OD	20/20 OU	

For control subjects, the primary diagnosis resulting in examination in the retina clinic is listed. N/A indicates subjects who were recruited as a control subject without any ocular complaint. ALT, alanine transaminase; AST, aspartate transaminase; BNH, black/non-Hispanic; CRVO, central retinal vein occlusion; OD, right eye; OS, left eye; OU, both eyes; PVD, posterior vitreous detachment; RA, rheumatoid arthritis; SLE, systemic lupus erythematosus; WNH, white/non-Hispanic.

OCT system described above, and a commercially available SS-OCT system (PLEX Elite; Carl Zeiss Meditec, Dublin, CA). Imaging on the SS-OCT was performed using a standard 6-mm × 6-mm raster

scan pattern centered on the fovea. VIS-OCT imaging was performed using high-definition (HD) four-line radial (32 × 2048 A-lines × 4 B-scans) and horizontal (64 × 1024 A-lines × 1 B-scan) line scans in the

region of the raster scan pattern from the SS-OCT and SD-OCT devices. Only the horizontal foveal scan was used for analyses from each scan pattern. This was achieved by averaging either 32 or 64 single B-scans into one HD B-scan. Speckle noise, which is random by nature, is reduced by averaging, leading to a significant improvement in the signal-to-noise ratio (SNR).²³ During horizontal (x -direction) scanning, the y -galvo moves up and down within a small range of 0.16 mm. This process, which we refer to as modulation, captures 32 or 64 A-lines at each x -location which are averaged to generate one point in the final B-scan. The radial scanning pattern utilizes a four-line radial scanning pattern with an angular interval of $\pi/4$ to cover different regions of retina. Each B-scan contains 2048 A-lines, and 32 modulated A-lines are averaged over ~ 0.2 mm orthogonally to the B-scan direction to enhance the signal and reduce noise.

In this study, the line rate was 100 kHz, the acquisition time for the four-line HD radial scanning pattern was 2.62 seconds per scan, and the single-line HD scan required 0.66 seconds per scan. Images were flattened using a custom algorithm. VIS-OCT and SS-OCT foveal scans were manually registered by using the depth of the foveal center.

Image Processing for VIS-OCT

We employed a per-A-line noise cancellation algorithm to eliminate the baseline light source spectrum, reduce noise, and enhance the SNR, as previously published.²² Dispersion compensation and fast Fourier transform (FFT) were then applied to generate B-scans. To establish the display range, we defined the intensity of the background after FFT as the lower boundary and selected the intensity value at 0.05% from the sorted values (from high to low) as the upper boundary. Utilizing these upper and lower boundaries, we applied a logarithmic scale and normalization for image display.

Given the substantial dynamic range (exceeding 60 dB for control subjects) between the inner and outer retina, achieving a balanced visual effect proved challenging. Adjustment of the brightness and contrast of the images for display (as shown in the figures) was guided by physician recommendations to ensure visibility of inner retinal structures, allowing for a more standardized presentation of B-scans. Therefore, we increased the image brightness by 40% to enhance the visibility of the inner retina, although this resulted in saturation of the outer retina, as illustrated in Figure 1 and Supplementary Figure S2. Additionally, we manually flattened the B-scans

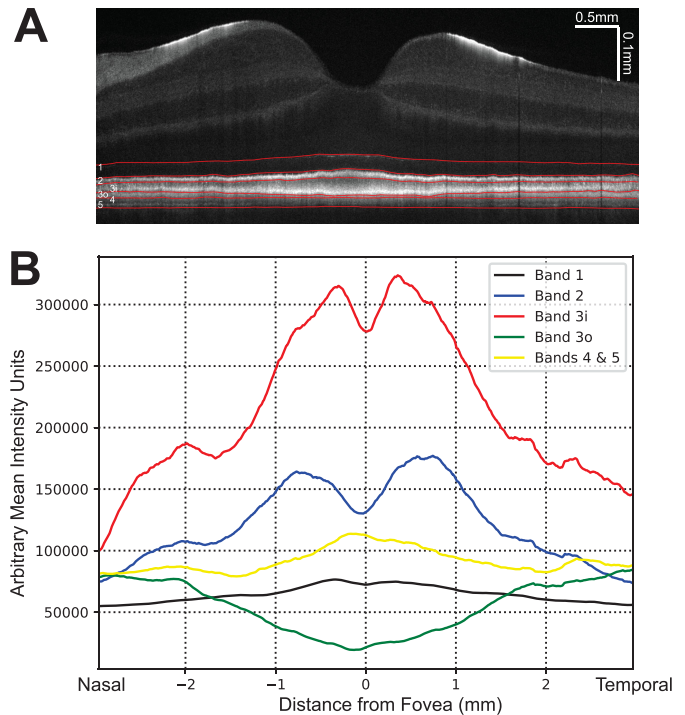


Figure 2. (A) VIS-OCT image of control subject demonstrating manual segmentation of outer retinal layers (red). (B) Mean intensity of each outer retinal band (summation of intensity between manually segmented outer retinal bands) averaged across three control subjects shown relative to distance from the foveal pit.

based on band 5 (BM) (Supplementary Fig. S1). The intensity of each outer retinal layer was quantified by manually segmenting the boundaries of each layer and calculating the cumulative intensity between the boundaries. The manual segmentation shown in Figure 2 was performed independently by two separate graders, and differences were adjudicated by a third grader. To compare parafoveal outer retinal band intensity (Figs. 3G, 4G, 5G), the average A-scan intensity from a region 3 to 6 mm eccentric from the fovea was compared between subjects taking HCQ and an average of the same regions in three control subjects (selected to correspond as closely as possible with the mean age of the HCQ group).

Results

As shown in the Table, a total of 20 eyes from 12 control subjects without known retinal pathology (mean age, 40 ± 22 years) were recruited into this study. VIS-OCT imaging of these subjects demonstrated outer retinal anatomy in finer detail than previously possible with conventional OCT technol-

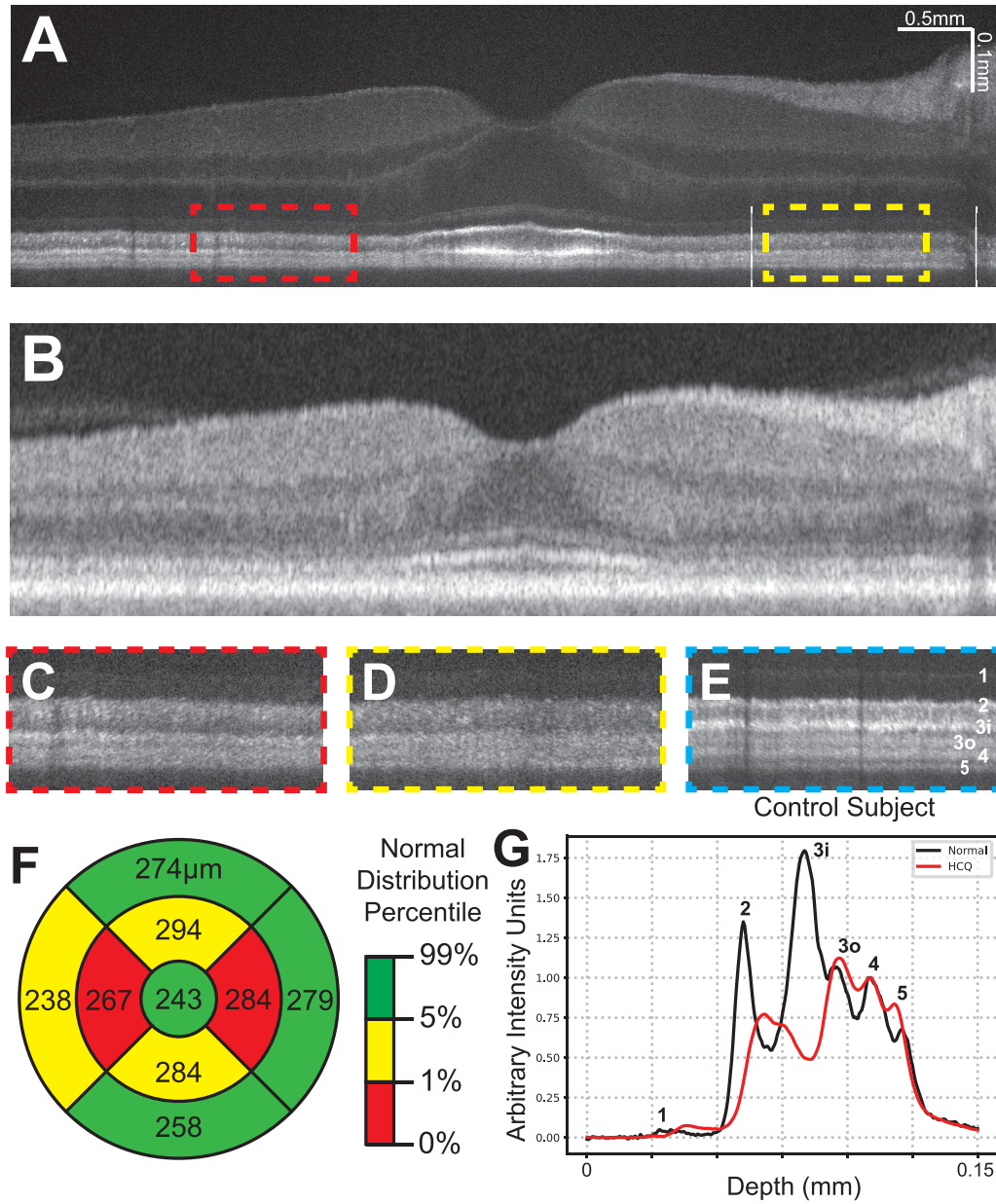


Figure 3. (A) Contrast-adjusted VIS-OCT image of a 62-year-old subject with a history of systemic lupus erythematosus and 11 years of HCQ use. (B) SS-OCT image of the same subject in panel a. (C, D) Magnified view of parafoveal outer retinal features (dashed lines in panel a) demonstrating broadening of band 2 and loss of layer 3i. (E) Magnified view of outer retinal features from control subject at distances to fovea as for panels c and d, scaled to align with panels c and d. (F) Central subfield thickness map of total retinal thickness obtained from SS-OCT; measurements are listed in micrometers. Coloring indicates normal distribution percentile per device manufacturer. (G) Averaged A-line signal over the nasal 3-mm to 6-mm eccentricity from panel a between two white lines in red. The averaged A-line trace signal from three control subjects (ages 35, 70, and 80 years; mean age, 62 ± 19 years) at the same eccentricity is shown in black. Both A-lines have zero means and were normalized to the RPE band.

ogy. Figure 1 and Supplementary Figure S2 show representative VIS-OCT images from control subjects. Within the foveola, five hyperreflective outer retinal bands were visualized, labeled as bands 1 to 5 (Fig. 1C). These bands were putatively identified as the external limiting membrane (ELM, band 1), EZ (band 2), cone outer segment tips (COST, band 3), RPE (band 4), and

BM (band 5). This banding pattern was observed in all control subjects irrespective of patient age. Henle’s fiber layer was visible as a slightly darker region above the outer nuclear layer (Figs. 1B, 1E). Magnified views of the inner plexiform layer revealed sublayers in the perifoveal region (Figs. 1B, 1F), consistent with previous findings.²⁴

In the parafoveal region, outer retinal band 3 consistently divided into two distinct hyperreflective bands, labeled band 3 inner (3i) and band 3 outer (3o), for a total of six hyperreflective bands (Figs. 1A, 1D). In accordance with prior anatomical studies and previously published VIS-OCT imaging data,^{14,22} these bands were putatively identified as the COST and rod outer segment tips (ROST), respectively. To better characterize these bands, each one was manually segmented, and the mean intensity of each band averaged across three control subjects was plotted as a function of the distance from the fovea (Fig. 2). Notably, the intensity of band 3i peaked in the foveal region and sharply declined with increasing retinal eccentricity. On the other hand, band 3o was not visible in the foveal region and gradually appeared with increasing retinal eccentricity. This pattern mirrors previously published histological studies of cone and rod density,^{25,26} supporting the hypothesis that bands 3i and 3o represent COST and ROST, respectively. This inverse relationship between bands 3i and 3o was consistent between two graders who independently segmented the layers (Supplementary Fig. S3).

A total of 20 eyes from 10 subjects (mean age, 62 ± 16 years) with a history of HCQ use were recruited (Table). These subjects demonstrated a range in severity of HCQ toxicity findings (including subjects with suspected toxicity or no evidence of toxicity on prior testing) and were imaged using VIS-OCT. These subjects ranged in age (33–84 years) and length of HCQ use (1–35 years). The mean age of the subjects with a history of HCQ use was higher than that of the control group ($P < 0.02$, Mann–Whitney U test). Therefore, to compare parafoveal outer retinal band intensities between these groups, the average A-scan intensity from a region 3 to 6 mm eccentric from the fovea was compared between subjects using HCQ and an average of the same regions in control subjects with mean age 62 ± 19 years (Figs. 3G, 4G, 5G). This mean age was selected to correspond as closely as possible with the mean age of the HCQ group given the relatively small sample size. The approximate cumulative lifetime HCQ dose was calculated, and each patient's most recent renal and hepatic function testing was recorded if available from their medical records.

Figure 3 illustrates data from a 62-year-old female subject with an 11-year history of HCQ use (cumulative dose, 1204.5 g) and qualitatively unremarkable SD-OCT and SS-OCT scans (Fig. 3B). The patient had excellent visual acuity (20/20 in both eyes) and denied any subjective vision changes at the time of examination. HCQ toxicity was suspected based on serial SD-OCT central subfield thickness measure-

ments showing decreasing thickness in the nasal and temporal Early Treatment Diabetic Retinopathy Study (ETDRS) subfield sectors (Figs. 3B, 3F), as described in Melles et al.⁶ VIS-OCT images (Figs. 3A, 3C, 3D) were compared to a control subject (Fig. 3E) and demonstrated blunting of most band boundaries, as well as essentially complete loss of band 3i in the parafoveal region. Figure 3G illustrates the average intensity profile of the outer retina in the nasal parafovea from 3-mm to 6-mm eccentricity, corresponding to the outer parafoveal ETDRS subfield (indicated with vertical white dashed lines in Fig. 3A). There was a marked decrease in the pixel intensity of regions corresponding to bands 2 and 3o (red line) relative to the average of three control subjects (black line, mean age 62 ± 19 years), as well as in comparison to the intensity of bands 4 and 5, suggestive of damage to the photoreceptor bands. This decrease in band reflectivity ($\sim 4\times$ decrease) was much larger proportionately than the qualitative decrease in the thickness from the ELM to BM illustrated in Figure 3G. Also, the mean retinal thickness from the same 3-mm to 6-mm nasal parafoveal ETDRS subfield was within the normal range relative to a normative database ($279 \mu\text{m}$ in Fig. 3F).

Figure 4 illustrates data from a 73-year-old female subject with a 5-year history of HCQ use (cumulative dose, 730 g) and excellent best-corrected visual acuity of 20/25 in the right eye and 20/20 in the left eye. She denied any subjective vision changes at the time of the examination. SD-OCT and SS-OCT images suggested a very mild parafoveal attenuation of the ELM and/or EZ. Serial SD-OCT central subfield thickness assessments suggested thinning in the nasal and temporal parafoveal ETDRS subfields (Fig. 4F), as described in Melles et al.⁶ These findings were concerning for early HCQ toxicity, and the patient was closely monitored and encouraged to minimize the dose of HCQ. VIS-OCT imaging demonstrated diffuse attenuation of band 3i and patchy parafoveal attenuation of band 3o, which were not clearly apparent on individual b-scans scans in commercially available devices (Figs. 4A vs. 4B) or in control subjects (Figs. 4C and 4D compared to Fig. 4E). Similar to the subject in Figure 3, there was a marked decrease in the intensity of the photoreceptor bands (particularly bands 3i and 3o) relative to the intensity of bands 4 and 5 (Fig. 4G). This decrease in band reflectivity was present despite any qualitative decrease in the thickness from the ELM to BM, as illustrated in Figure 4G. The subject ultimately stopped HCQ use due to the significant concern for early toxicity. An additional example of suspected HCQ toxicity is demonstrated in Supplementary Figure S4A.

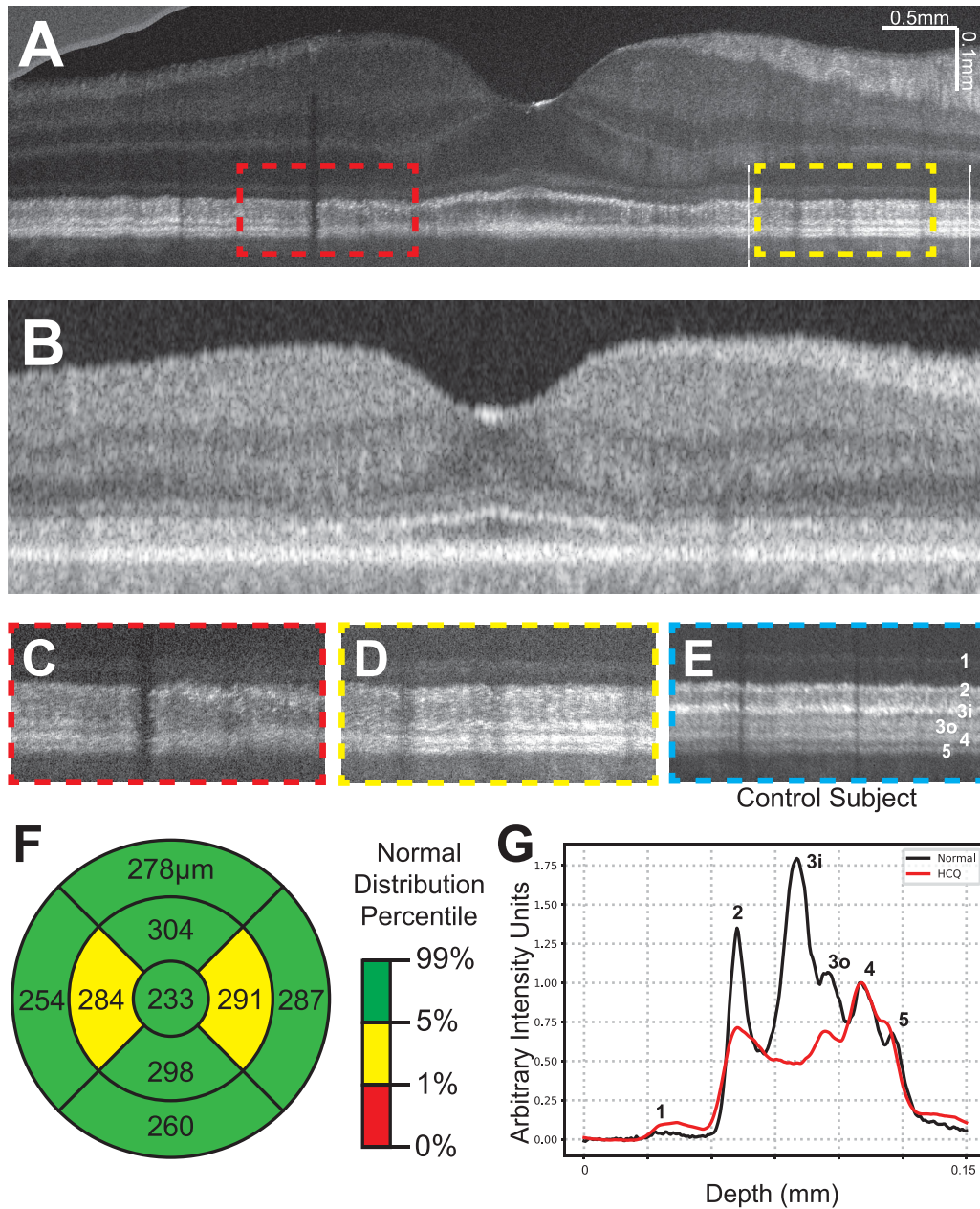


Figure 4. (A) Contrast-adjusted VIS-OCT image of 73-year-old patient with a 5-year history of HCQ use and suspected HCQ retinal toxicity. (B) SS-OCT image of same subject in panel a. (C, D) Magnified view of parafoveal outer retinal features (*dashed lines* in panel a) demonstrating broadening of band 2, loss of band 3i, and patchy attenuation of band 3o. (E) Magnified view of outer retinal features from a control subject at distances to the fovea similar to panels c and d, scaled to align with panels c and d. (F) Central subfield thickness map of total retinal thickness obtained from SS-OCT; measurements are listed in micrometers. (G) Averaged A-line signal over the nasal 3-mm to 6-mm eccentricity from panel A between two *white lines*. The averaged A-line trace signal from three control subjects (ages 35, 70, and 80 years; mean age, 62 ± 19 years) at the same eccentricity is shown in *black*. Both A-lines have zero means and were normalized to the RPE band.

VIS-OCT imaging of subjects with symptomatic and severe HCQ retinal toxicity demonstrated marked parafoveal attenuation of bands 2, 3i, 3o, and 4 (Fig. 5A) in a 53-year-old subject with a 4-year history of HCQ use (cumulative dose, 584 g). Given the severity of damage, this attenuation was also evident with SS-

OCT (Fig. 5B) and with a marked decrease in SD-OCT central subfield retinal thickness, as well (Fig. 5F). At the time of imaging, the patient's best-corrected visual acuity was 20/63 in the right eye and 20/80 in the left eye, and the patient had been previously diagnosed with severe HCQ toxicity. The medication had been discon-

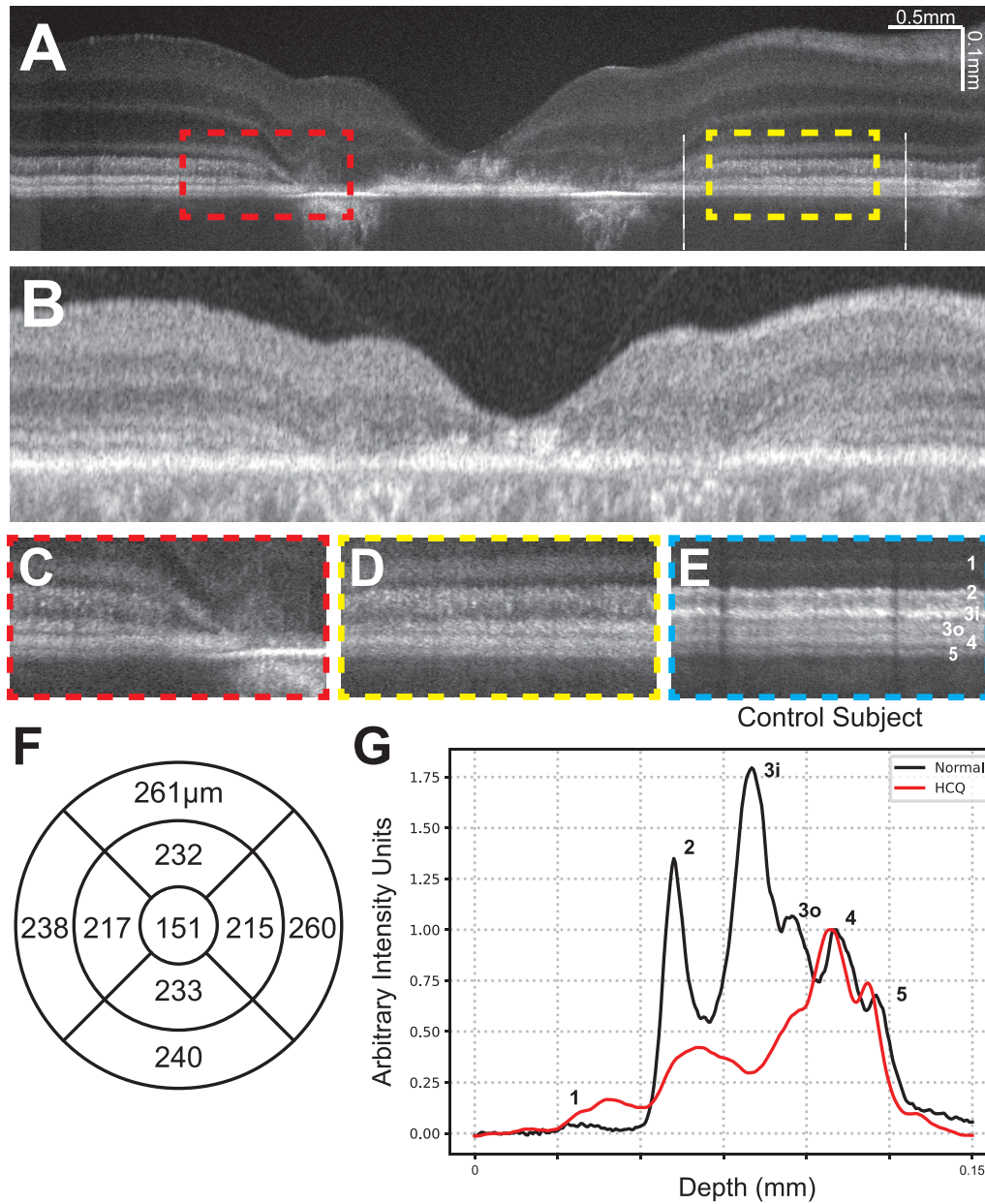


Figure 5. (A) Contrast-adjusted VIS-OCT image of 53-year old patient with a 4-year history of HCQ use with severe HCQ retinal toxicity and no other known retinal pathology. (B) SS-OCT image of the same subject in panel a. (C, D) Magnified view of parafoveal outer retinal features (dashed lines in panel a) demonstrating diffuse loss of bands 2, 3i, 3o, and 4. (E) Magnified view of outer retinal features from a control subject at distances to the fovea similar to panels c and d, scaled to align with panels c and d. (F) Central subfield thickness map of total retinal thickness obtained from SS-OCT; measurements are listed in micrometers. Comparison to normative data was not available from the device manufacturer. (G) Averaged A-line signal over the nasal 3-mm to 6-mm eccentricity from panel A between two white lines. The averaged A-line trace signal from three control subjects (ages 35, 70, and 80 years; mean age, 62 ± 19 years) at the same eccentricity is shown in black. Both A-lines have zero means and were normalized to the RPE band.

tinued prior to our examination. Notably, even in this subject, there was more severe attenuation of band 3i compared to any other band, with increasing eccentricity beyond the parafovea where clear atrophy was not evident. Although all bands were less distinct than normal, bands 1, 2, and 3o were particularly diffuse

when compared with a control subject (Figs. 5C and 5D vs. 5E). In no case was the attenuation of any band more severe than the attenuation of band 3i (Fig. 5G). As in the previous case, this decrease in band reflectivity was present despite any qualitative decrease in the thickness from the ELM to BM, as illustrated in

Figure 5G. An additional example of severe HCQ toxicity is provided in Supplementary Figure S4B.

Discussion

Using ultrahigh-resolution VIS-OCT, we demonstrated outer retinal banding patterns that are not clearly or reliably visible with commercially available SD-OCT or SS-OCT. Most importantly, these changes in banding pattern reflectivity are much larger in magnitude than changes in retinal thickness measured qualitatively or quantitatively on SD-OCT or SS-OCT. We also demonstrated that the outer retinal band intensity profiles on VIS-OCT in the healthy controls were similar to the known density profiles of rods and cones from histologic studies. In control subjects, we consistently identified five outer retinal bands in the foveola (bands 1, 2, 3, 4, and 5) and six bands in the parafovea (bands 1, 2, 3i, 3o, 4, and 5). These bands putatively represent (1) the ELM, (2) the EZ, (3i) the COST, (3o) the ROST, (4) the RPE, and (5) BM. These data strongly suggest that VIS-OCT imaging can distinguish rod- and cone-specific image features non-invasively.

We also demonstrated the utility of ultrahigh-resolution VIS-OCT to detect subclinical changes in the outer retinal band reflectivity corresponding to photoreceptor outer segments in asymptomatic subjects at high risk of HCQ toxicity. Specifically, we observed that band 3i (corresponding to the putative COST) was consistently and most severely attenuated in subjects at high risk of toxicity and in whom serial SD-OCT measurements from commercial devices demonstrated retinal thinning. Attenuation of band 3i was visible in all subjects with suspected or known toxicity. Notably, attenuation of band 3i was not seen in subjects without any other evidence of toxicity, and this finding of serial thinning has been implicated in HCQ toxicity.⁶ We hypothesize that attenuation of band 3i is the earliest sign of HCQ toxicity and may be readily detectable on a single-visit VIS-OCT, whereas serial SD-OCT measurements over months or years are needed to detect decreasing thickness trends. In our individual VIS-OCT scans, the attenuation of VIS-OCT banding reflectivity was present despite normal retinal thickness as measured with central subfield thickness using SD-OCT when compared with age-matched control subjects. We hypothesize that this outer retinal attenuation of band 3i is the earliest known marker of HCQ toxicity. Our analyses assessing the cumulative intensity of bands 3i and 3o at increasing retinal eccentrici-

ties in **Figure 2** closely align with previously published anatomical studies quantifying cone and rod densities,²⁵ supporting the hypothesis that these bands represent the cone and rod photoreceptor outer segments, respectively.

The mechanism of HCQ retinopathy is not clearly understood, although prior studies have suggested multiple potential mechanisms.²⁷ A study by Xu et al.²⁸ demonstrated that both chloroquine and HCQ inhibit organic anion-transporting peptide 1A2 (OATP1A2), which mediates uptake of all-*trans*-retinoic acid in the RPE in the visual cycle. This may lead to toxicity of both photoreceptors, as well as the RPE. Animal studies have revealed the binding of chloroquine to pigmented retinal structures, including the RPE.²⁹ It is unclear why band 3i appeared to be attenuated first in subjects on HCQ followed by band 3o, although this finding suggests a tendency for cone photoreceptors to be preferentially lost over rods. In more severe stages, as shown in **Figure 5**, there appears to be attenuation of the remaining outer retinal bands, including the RPE, favoring a mechanism of toxicity affecting both the RPE and the photoreceptors.

Recent work has measured EZ attenuation with SD-OCT to detect and quantify HCQ toxicity.^{30,31} Our results demonstrate the ability of VIS-OCT imaging to detect early HCQ toxicity with attenuation of the photoreceptor bands, which are not easily visible with SD-OCT or SS-OCT, prior to EZ attenuation. We demonstrated that early HCQ toxicity is characterized mainly by attenuation of bands 3i and 3o, with more severe toxicity affecting the EZ and the RPE. This corroborates earlier studies suggesting that damage occurs to the photoreceptors.^{4,29} As demonstrated in **Figures 3** and **4**, early toxicity is often not apparent on individual line scans with SS-OCT (or SD-OCT), requiring averaging of retinal thickness across a large region to observe retinal thinning on serial thickness maps. Using VIS-OCT, these changes are apparent on foveal line scans and may assist with earlier diagnosis of HCQ toxicity.

It is important to note that there are limitations to VIS-OCT imaging compared to SS-OCT and conventional U.S. Food and Drug Administration–approved devices. First, the brightness of the visible light used to acquire VIS-OCT images can be distracting to patients, particularly when utilizing lengthy imaging protocols or in patients who are light sensitive. Additionally, although its increased resolution allows for visualization of BM, visible light is limited in its ability to penetrate beyond BM and visualize structures within the choroid, which may limit its utility in the diagnosis of choroidal pathologies. Ultrahigh-resolution SD-OCT has also recently demonstrated the ability to

reveal finer features of the outer retina than previously possible with conventional imaging techniques, including the separate hyperreflective bands corresponding to the RPE and BM.³² However, the finer axial resolution of VIS-OCT enables unique contrast and clearer separation between layers. Furthermore, another advantage and potential application of VIS-OCT lies in its retinal oximetry capability, which is not possible with NIR-OCT due to the higher absorption and scattering contrast between oxygenated and deoxygenated hemoglobin in the visible light wavelength range.

This study examined the early results of an ongoing investigation studying the early detection of HCQ toxicity using VIS-OCT, as well as the relationship between HCQ use and outer segment reflectivity. Of note, the average age of the control subjects was younger than the average age of the HCQ group. However, the marked changes visualized in the reflectivity of band 3i were not qualitatively present in older control subjects (Supplementary Fig. S5) or in the average intensity profile of three control subjects with mean age very similar to the mean age of the HCQ group (Figs. 3G, 4G, 5G). Due to our small sample size, it remains unclear whether the pattern of changes described can also be seen in other retinal diseases or whether they are specific to HCQ toxicity, but it is unlikely that it is due to age alone.

Our findings support previous work suggesting that anatomically detectable damage to photoreceptors precedes similar damage to the RPE.^{1,4} Prospective studies and analyses with larger sample sizes will be necessary to further characterize these changes. Previous studies have demonstrated that subjects of Asian heritage often demonstrate an extramacular pattern of damage.¹ Additional work is necessary to determine whether VIS-OCT can demonstrate this difference or provide further insight into its pathogenesis. Prior work has also demonstrated that, in a minority of patients, early HCQ toxicity is detected on visual field testing prior to clear SD-OCT changes, although this is likely due to the limited resolution of single SD-OCT scans to reliably demonstrate changes in the outer retinal layers as we have shown above.³³ Further work with a larger sample size is necessary to determine whether changes on VIS-OCT can reliably be detected prior to visual field changes.

Acknowledgments

Supported by grants from the National Institutes of Health (R01NS108464, R01EY032163, and

R01EY034607 to JY), and by a Boone Pickens Professorship in Ophthalmology (AHK).

Disclosure: **A.K. Garg**, None; **J. Wang**, None; **B. Alonzo**, None; **J. Yi**, None; **A.H. Kashani**, Carl Zeiss Meditec (C), Aspen Biosciences (C), RegenXBio (C), Alcon (C)

* AKG and JW contributed equally to this article.

References

- Marmor MF, Kellner U, Lai TYY, Melles RB, Mieler WF. Recommendations on screening for chloroquine and hydroxychloroquine retinopathy (2016 revision). *Ophthalmology*. 2016;123(6):1386–1394.
- Gonasun LM, Potts AM. In vitro inhibition of protein synthesis in the retinal pigment epithelium by chloroquine. *Invest Ophthalmol*. 1974;13(2):107–115.
- Sundelin SP, Terman A. Different effects of chloroquine and hydroxychloroquine on lysosomal function in cultured retinal pigment epithelial cells. *APMIS*. 2002;110(6):481–489.
- Marmor MF. Comparison of screening procedures in hydroxychloroquine toxicity. *Arch Ophthalmol*. 2012;130(4):461–469.
- Ruberto G, Bruttini C, Tinelli C, Cavagna L, Bianchi A, Milano G. Early morpho-functional changes in patients treated with hydroxychloroquine: a prospective cohort study. *Graefes Arch Clin Exp Ophthalmol*. 2018;256(11):2201–2210.
- Melles RB, Marmor MF. Rapid macular thinning is an early indicator of hydroxychloroquine retinal toxicity. *Ophthalmology*. 2022;129(9):1004–1013.
- Ugwuegbu O, Uchida A, Singh RP, et al. Quantitative assessment of outer retinal layers and ellipsoid zone mapping in hydroxychloroquine retinopathy. *Br J Ophthalmol*. 2019;103(1):3–7.
- Barnes AC, Bhavsar KV, Weber ML, Witkin AJ. A subtle case of hydroxychloroquine retinopathy: spectral domain optical coherence tomography findings. *Eye (Lond)*. 2014;28(12):1521–1522.
- Kim KE, Ahn SJ, Woo SJ, et al. Use of OCT retinal thickness deviation map for hydroxychloroquine retinopathy screening. *Ophthalmology*. 2021;128(1):110–119.
- De Sisternes L, Hu J, Rubin DL, Marmor MF. Analysis of inner and outer retinal thickness in patients using hydroxychloroquine prior to

- development of retinopathy. *JAMA Ophthalmol.* 2016;134(5):511–519.
11. Yi J, Wei Q, Liu W, Backman V, Zhang HF. Visible-light optical coherence tomography for retinal oximetry. *Opt Lett.* 2013;38(11):1796–1798.
 12. Chong SP, Bernucci M, Radhakrishnan H, Srinivasan VJ. Structural and functional human retinal imaging with a fiber-based visible light OCT ophthalmoscope. *Biomed Opt Express.* 2017;8(1):323–337.
 13. Zhang T, Kho AM, Yiu G, Srinivasan VJ. Visible light optical coherence tomography (OCT) quantifies subcellular contributions to outer retinal band 4. *Transl Vis Sci Technol.* 2021;10(3):30.
 14. Srinivasan VJ, Kho AM, Chauhan P. Visible light optical coherence tomography reveals the relationship of the myoid and ellipsoid to band 2 in humans. *Transl Vis Sci Technol.* 2022;11(9):3.
 15. Shu X, Beckmann L, Wang Y, et al. Designing visible-light optical coherence tomography towards clinics. *Quant Imaging Med Surg.* 2019;9(5):769–781.
 16. Yi J, Chen S, Shu X, Fawzi AA, Zhang HF. Human retinal imaging using visible-light optical coherence tomography guided by scanning laser ophthalmoscopy. *Biomed Opt Express.* 2015;6(10):3701–3713.
 17. Chauhan P, Kho AM, FitzGerald P, Shibata B, Srinivasan VJ. Subcellular comparison of visible-light optical coherence tomography and electron microscopy in the mouse outer retina. *Invest Ophthalmol Vis Sci.* 2022;63(9):10.
 18. Chauhan P, Kho AM, Srinivasan VJ. From soma to synapse: imaging age-related rod photoreceptor changes in the mouse with visible light OCT. *Ophthalmol Sci.* 2023;3(4):100321.
 19. Wang J, Nolen S, Song W, Shao W, Yi W, Yi J. Second-generation dual-channel visible light optical coherence tomography enables wide-field, full-range, and shot-noise limited retinal imaging. bioRxiv. 2022, <https://doi.org/10.1101/2022.10.05.511048>.
 20. Won J, Takahashi H, Ploner SB, et al. Topographic measurement of the subretinal pigment epithelium space in normal aging and age-related macular degeneration using high-resolution OCT. *Invest Ophthalmol Vis Sci.* 2024;65(10):18.
 21. Reche J, Stocker AB, Henchoz V, et al. High-resolution optical coherence tomography in healthy individuals provides resolution at the cellular and subcellular levels. *Transl Vis Sci Technol.* 2023;12(7):12.
 22. Wang J, Nolen S, Song W, et al. A dual-channel visible light optical coherence tomography system enables wide-field, full-range, and shot-noise limited human retinal imaging. *Commun Eng.* 2024;3(1):21.
 23. Rubinoff I, Beckmann L, Wang Y, et al. Speckle reduction in visible-light optical coherence tomography using scan modulation. *Neurophoton.* 2019;6(4):041107.
 24. Zhang T, Kho AM, Srinivasan VJ. In vivo morphometry of inner plexiform layer (IPL) stratification in the human retina with visible light optical coherence tomography. *Front Cell Neurosci.* 2021;15:655096.
 25. Curcio CA, Sloan KR, Kalina RE, Hendrickson AE. Human photoreceptor topography. *J Comp Neurol.* 1990;292(4):497–523.
 26. Song H, Chui TYP, Zhong Z, Elsner AE, Burns SA. Variation of cone photoreceptor packing density with retinal eccentricity and age. *Invest Ophthalmol Vis Sci.* 2011;52(10):7376.
 27. Yusuf IH, Sharma S, Luqmani R, Downes SM. Hydroxychloroquine retinopathy. *Eye (Lond).* 2017;31(6):828–845.
 28. Xu C, Zhu L, Chan T, et al. Chloroquine and hydroxychloroquine are novel inhibitors of human organic anion transporting polypeptide 1A2. *J Pharmaceut Sci.* 2016;105(2):884–890.
 29. Rosenthal R, Kolb H, Bergsma D, Huxsoll D, Hopkins JL. Chloroquine retinopathy in the rhesus monkey. *Invest Ophthalmol Vis Sci.* 1978;17(12):1158–1175.
 30. Kalra G, Talcott KE, Kaiser S, et al. Machine learning-based automated detection of hydroxychloroquine toxicity and prediction of future toxicity using higher-order OCT biomarkers. *Ophthalmol Retina.* 2022;6(12):1241–1252.
 31. De Silva T, Jayakar G, Grisso P, Hotaling N, Chew EY, Cukras CA. Deep learning-based automatic detection of ellipsoid zone loss in spectral-domain OCT for hydroxychloroquine retinal toxicity screening. *Ophthalmol Sci.* 2021;1(4):100060.
 32. Chen S, Abu-Qamar O, Kar D, et al. Ultrahigh resolution OCT markers of normal aging and early age-related macular degeneration. *Ophthalmol Sci.* 2023;3(3):100277.
 33. Marmor MF, Melles RB. Disparity between visual fields and optical coherence tomography in hydroxychloroquine retinopathy. *Ophthalmology.* 2014;121(6):1257–1262.